Modeling of CO2 Stripping in a Hollow Fiber Membrane Contactor for CO2 Capture

ARTICLE *in* ENERGY & FUELS · OCTOBER 2013

Impact Factor: 2.79 · DOI: 10.1021/ef401488c

5 AUTHORS, INCLUDING:

Zhen Wang
Qingdao University
15 PUBLICATIONS **196** CITATIONS
SEE PROFILE

Hai Yu
The Commonwealth Scientific and Industrial …
57 PUBLICATIONS **443** CITATIONS
SEE PROFILE

Zhongyang Luo
Zhejiang University
242 PUBLICATIONS **2,926** CITATIONS
SEE PROFILE

energy&fuels

Article

pubs.acs.org/EF

Modeling of CO_2 Stripping in a Hollow Fiber Membrane Contactor for CO_2 Capture

Zhen Wang,[†,‡] Mengxiang Fang,*[,†] Hai Yu,[‡] Qinhui Ma,[†] and Zhongyang Luo[†]

[†]State Key Laboratory of Clean Energy Utilization, Zhejiang University, Hangzhou 310027, People's Republic of China

[‡]CSIRO Energy Centre, Mayfield West, NSW 2304, Australia

ABSTRACT: Membrane stripping is a promising method for carbon dioxide (CO_2) desorption with low energy demand. We developed a mathematical model to simulate the CO_2 stripping from the CO_2-rich monoethanolamine (MEA) solvent in a hollow fiber membrane contactor. The modeling results agreed well with literature experimental results. To improve the understanding and facilitate the optimization of the membrane based CO_2 stripping process, we investigated the effects of different operating variables including liquid flow velocity, sweeping gas flow rate, regeneration pressure, and temperature on CO_2 desorption performance. The effects of membrane's length and diameter of membrane fiber on CO_2 desorption were also studied. Results showed that increasing membrane's length will improve CO_2 stripping performance, but not infinitely, because of the thermodynamic limitation of absorbent, and shorter membrane module is preferred for thinner membrane. Membranes with a smaller diameter favor CO_2 desorption. To predict the influence of membrane wetting on CO_2 stripping performance, the change of CO_2 lean loading with the wetting ratio was investigated. Membrane wetting significantly deteriorates CO_2 membrane desorption performance, with CO_2 lean loading increasing suddenly once the membrane is wetted.

1. INTRODUCTION

The excessive emission of carbon dioxide (CO_2), resulting from the expansion of industrial activities such as massive coal-fired power generation, is significantly contributing to global warming.[1] Hence, reduction of CO_2 emissions from the coal-fired power stations and many other sources has become a challenging but crucial issue to mitigate climate change.[2] Currently, CO_2 separation by amine-based solvents is considered to be the most promising method for CO_2 capture from flue gas in power stations.[3−5] This is due to its successful commercial applications in many industries; its effectiveness for gas streams of low CO_2 partial pressure; and its tail-end technology, which can be retrofitted to existing power plants.[5] However, this technology is energy-intensive and consumes a significant amount of heat for solvent regeneration, reducing the power plant efficiency by as much as 30%.[6,7]

To address this problem, different stripper configurations were proposed to minimize the regeneration energy. Oyenekan et al.[8] evaluated four innovative stripper configurations and found that the matrix stripper had the lowest energy consumption. Van Wagener et al.[9] compared five different stripper configurations and found that the reduction of energy consumption by 9%−11% was achieved with the interheated column stripper. However, all these improvements from variation of stripper configurations come at the expense of complexity and capital cost. On the other hand, these improvements are still based on conventional packed columns and cannot avoid some operating problems such as foaming, flooding, channeling, and entrainment in the stripper.[10]

Membrane contactors were proposed as a promising alternative to conventional packed columns for the CO_2 absorption/stripping process and have been studied over past few decades.[11−14] Because of their high interfacial area per volume and membrane functions, they can provide superior process efficiency and potentially reduce capital cost and operational cost, compared to conventional packed columns.[12,15] In addition, most of operating problems associated with a packed tower can be overcome by using membrane contactors, becasue of nondispersive gas−liquid contact via a porous membrane.[16]

Although CO_2 absorption using membrane contactors has been extensively studied, reports on CO_2 stripping using membrane contactors are relatively rare in the open literatures. Figure 1 gives a typical process flow diagram of CO_2 absorption−membrane stripping process. The solvents after CO_2 absorption enter into the lumen side of the membrane contactors, and the water steam sweeps through the shell side of the membrane contactors by the driving force of the vacuum pump. The CO_2 and steam leaving the membrane strippers pass into a condensate reflux section to separate each other with condensed water being recycled. In this process, the regeneration temperature, which is usually ∼353 K, is lower than conventional thermal regeneration temperature. Lower regeneration temperature means that low-grade steam extracted from the turbine can be utilized to regenerate the solvent, which has the potential to reduce energy penalty for the power plant. Kosaraju et al.[17] investigated the continuous CO_2 absorption-stripping using commercial PP membrane contactors for an extended period of 55 days. A stable performance of membrane with long-term operation demonstrated the feasibility of CO_2 stripping in membrane contactor. Khaisri et al.[18] tested the CO_2 desorption performance and stability of the polytetrafluoroethylene (PTFE) hollow fiber membranes by using monoethanolamine (MEA) solution as the absorbent and

Received: July 30, 2013
Revised: September 30, 2013
Published: October 1, 2013

dx.doi.org/10.1021/ef401488c | *Energy Fuels* 2013, 27, 6887−6898

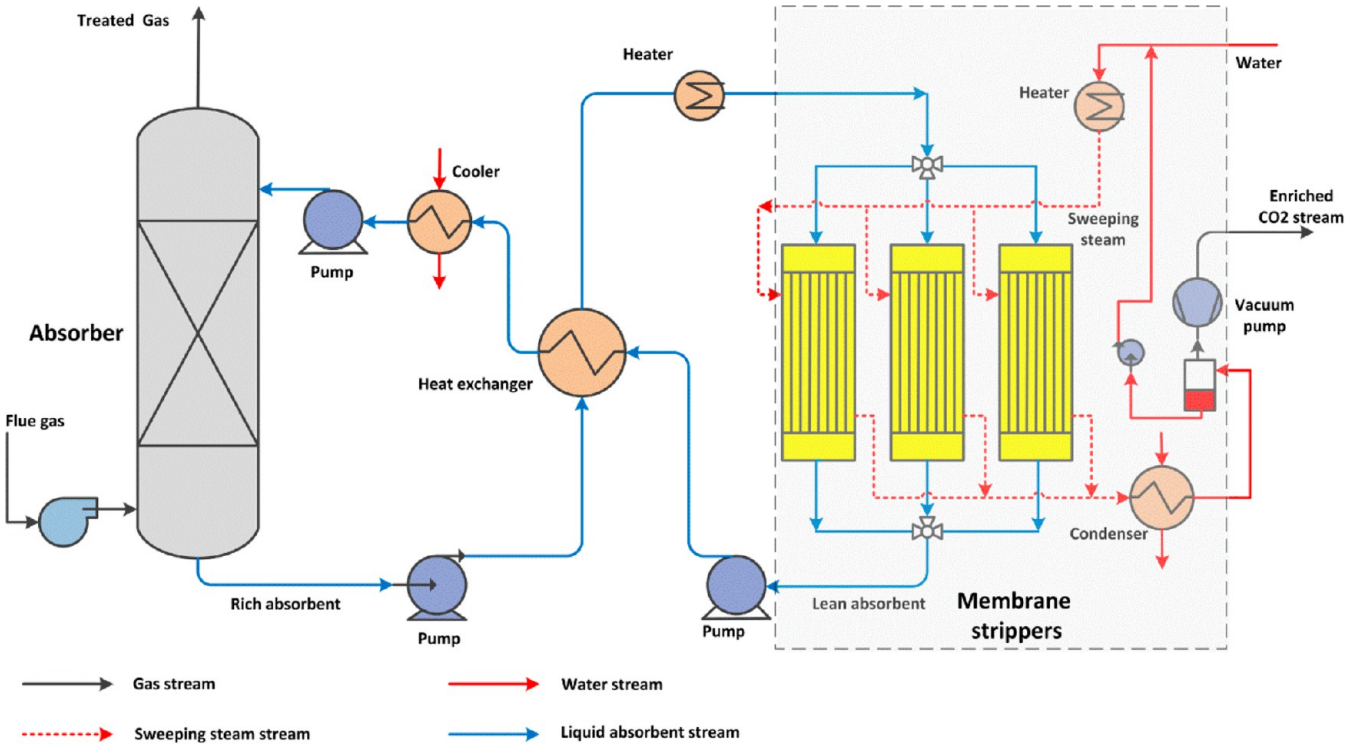

Figure 1. Typical flow sheet of CO_2 absorption–membrane stripping process.

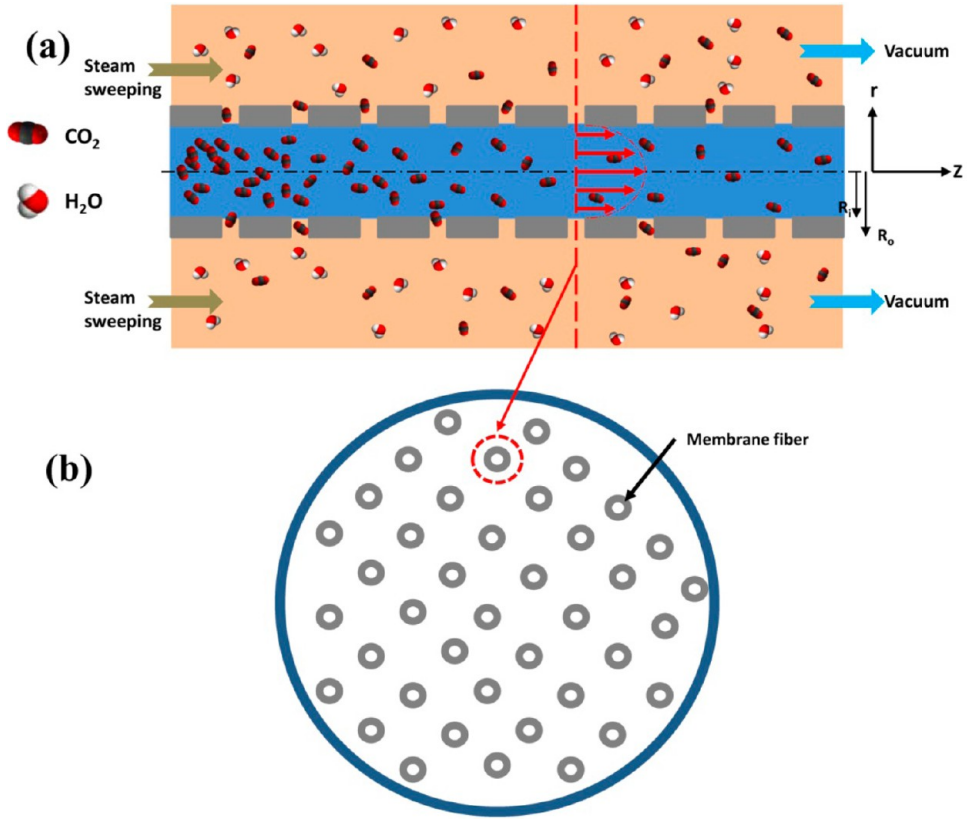

Figure 2. (a) Schematic diagram of the CO_2 stripping process in a hollow fiber membrane. (b) Cross section of the hollow fiber membrane contactor.

N_2 gas as the sweeping gas. Fang et al.[19,20] did similar work in a polypropylene (PP) hollow fiber membrane contactor. Water steam sweeping and vacuum operation in the gas side were employed together to strengthen the mass transfer of CO_2 desorption. Their studies showed that the membrane stripping process consumed lower total equivalent work than the thermal

dx.doi.org/10.1021/ef401488c | Energy Fuels 2013, 27, 6887–6898

regeneration in the packed column. Some novel membranes were also developed for CO_2 membrane stripping. Simioni et al.[21] used a symmetric polysulfone (PSf) with a hydrophobic surface coating for CO_2 desorption from aqueous potassium carbonate solvent. Koonaphapdeelert et al.[22] developed a ceramic hollow fiber membrane contactor, which has advanced chemical and thermal stability, for CO_2 stripping from MEA.

However, previous works have all focused on the experimental studies of CO_2 stripping in membrane contactors. To the best of our knowledge, there are very limited studies on modeling the membrane based stripping process in the open literature. For the purpose of gaining an improved understanding and facilitating the optimization of CO_2 membrane stripping process, a simulation work on CO_2 stripping in membrane contactors is necessary.

In the present work, we developed a mathematic model and used it to numerically simulate the process of CO_2 membrane stripping. In this process, 20 wt % MEA solvent with CO_2 loading of 0.5 mol CO_2/mol MEA was used as the rich solvent and flowed through the tube side of membrane contactor. Water steam, employed as a sweeping gas, flowed in the shell side. The pressure of the shell side was controlled by a vacuum pump. The effects of different operating variables including liquid flow velocity, sweeping gas flow rate, pressure and temperature, and structure characteristics of membrane fiber on CO_2 desorption were investigated. To predict the influence of membrane wetting on CO_2 stripping performance, the membrane wetting issue was also discussed in this work.

2. NUMERICAL MODEL DEVELOPMENT

2.1. Diffusion Reaction Governing Equations. The schematic diagram of CO_2 transport in the membrane stripping process is shown in Figure 2. Aqueous CO_2-rich solvent (e.g., MEA) is fed into the lumen side of the membrane contactor, while the water steam acts as sweeping gas flows through the shell side. The entire membrane contactor was immersed into a water bath and operated isothermally. In order to strengthen the mass transfer of CO_2 desorption, vacuum operation is also employed in the shell side to further decrease the CO_2 partial pressure in the gas phase. The CO_2 molecules will be desorbed from the CO_2-rich solution by permeating the gas-filled membrane pores from the lumen side to the shell side. In the mathematical model of CO_2 membrane stripping, the following assumptions were applied: (1) steady and isothermal state in operation; (2) a fully developed laminar parabolic velocity profile is applied in tube side; (3) negligible axial dispersion in the tube side; (4) Henry's law applicable in the gas/liquid interface; and (5) negligible pressure drop in the shell side.

Based on above assumptions, the steady-state continuity equations for each species with simultaneous diffusion and chemical reaction in the tube side can be expressed as

$$V_Z\frac{\partial[\mathrm{CO_2}]}{\partial Z} = D_{\mathrm{CO_2}}\left(\frac{\partial^2[\mathrm{CO_2}]}{\partial r^2} + \frac{1}{r}\frac{\partial[\mathrm{CO_2}]}{\partial r}\right) - r_{\mathrm{CO_2}} \quad (1)$$

$$V_Z\frac{\partial[\mathrm{MEA}]}{\partial Z} = D_{\mathrm{MEA}}\left(\frac{\partial^2[\mathrm{MEA}]}{\partial r^2} + \frac{1}{r}\frac{\partial[\mathrm{MEA}]}{\partial r}\right) - r_{\mathrm{MEA}} \quad (2)$$

where V_Z is the liquid velocity in the axial direction; $[CO_2]$ and [MEA] are, respectively, the free CO_2 and MEA concentrations in the liquid; D_{CO_2} and D_{MEA} are, respectively, the CO_2 and MEA diffusion coefficients in the liquid; and r_{CO_2} and r_{MEA} are the respective CO_2 and MEA reaction rates. Their specific calculations are presented in section 2.2.

The velocity profile in the tube side can be assumed to follow Newtonian laminar flow:

$$V_Z = 2\bar{V}\left[1 - \left(\frac{r}{R_i}\right)^2\right] \quad (3)$$

where $\bar{V}$ is the liquid mean velocity; and R_i is the inner radius of the membrane fiber.

The initial and boundary conditions for each component can be expressed as

$$[\mathrm{CO_2}] = 0,\ [\mathrm{MEA}] = [\mathrm{MEA}]_0 \qquad \text{for } Z = 0 \quad (4)$$

$$\frac{\partial[\mathrm{CO_2}]}{\partial r} = 0,\ \frac{\partial[\mathrm{MEA}]}{\partial r} = 0 \qquad \text{for } r = 0 \quad (5)$$

$$\frac{\partial[\mathrm{CO_2}]}{\partial r} = \frac{k_{\mathrm{ex}}(C_{\mathrm{CO_2,G}} - C^i_{\mathrm{CO_2,L}}/m)}{D_{\mathrm{CO_2}}},\ \frac{\partial[\mathrm{MEA}]}{\partial r} = 0 \qquad \text{for } r = R_i \quad (6)$$

where $[MEA]_0$ is the free MEA concentration in the liquid phase at the initial time, which is the function of MEA concentration, temperature, and CO_2 loading. It can be determined by the VLE model presented in section 2.3. $C_{CO_2,G}$ is the CO_2 bulk concentration in gas phase, $C^i_{CO_2,L}$ is the CO_2 liquid phase concentration in the gas/liquid interface, m is the distribution coefficient between the liquid and the gas, k_{ex} is the combination of mass transfer coefficients in the membrane and gas, $k_{ex} = 1/(1/k_g + 1/k_m)$.

As the membrane is operated without the pore wetting, the membrane mass-transfer coefficient, k_m, can be expressed as[23]

$$\frac{1}{k_{\mathrm{m}}} = \frac{\tau\delta}{D^e_{ig}\varsigma} \quad (7)$$

When partial wetting of the membrane occurs, the equation for k_m can change to

$$\frac{1}{k_{\mathrm{m}}} = \frac{(1-\phi)\tau\delta}{D^e_{ig}\varsigma} + \frac{\phi\tau\delta}{D_{\mathrm{CO_2,L}}\varsigma} \quad (8)$$

where ς is the membrane porosity; D^e_{ig} is the effective membrane diffusion coefficient in pure-gas-filled pores, and its detailed calculation is available in the Appendix; δ is the membrane thickness and τ is the tortuosity ($\tau = 1/\varsigma^2$); ϕ is the membrane pore wetting ratio; and $D_{CO_2,L}$ represents the diffusion coefficient of CO_2 in the liquid phase.

The gas-phase mass-transfer coefficient (k_g) can be predicted by the following equation:[24]

$$Sh = 5.85(1-\varphi)\left(\frac{d_{\mathrm{h}}}{L}\right)Re^{0.6}Sc^{0.33} \qquad 0.04 < \varphi < 0.4 \quad (9)$$

where φ is the packing density, L is the membrane fiber length; d_h is the hydraulic diameter of the shell side; and Re and Sc are the Reynolds and Schmidt numbers, respectively.

2.2. Reaction Scheme. The reaction of CO_2 with MEA can be described by a two-step zwitterionic mechanism.[25] The first

dx.doi.org/10.1021/ef401488c | Energy Fuels 2013, 27, 6887−6898

step of the reaction is to form a zwitterion as an intermediate, which can be expressed as

$$CO_2 + R_1R_2NH \underset{k_{-1}}{\overset{k_{2,Amine}}{\rightleftharpoons}} R_1R_2NH^+COO^- \quad (10)$$

The zwitterion then undergoes deprotonation by a base B:

$$R_1R_2NH^+COO^- + B \overset{k_b}{\rightarrow} R_1R_2NCOO^- + BH^+ \quad (11)$$

where B could be MEA, OH^-, or H_2O. The contribution of OH^- can usually be ignored, because of its very low concentration in solution.

For this mechanism, the CO_2 reaction rate and MEA reaction rate at quasi-steady state can be expressed as

$$r_{CO_2} = \frac{k_{2,MEA}[MEA]([CO_2] - [CO_2]_e)}{1 + \frac{k_{-1}}{k_{H_2O}[H_2O] + k_{MEA}[MEA]}} \quad (12)$$

$$r_{MEA} = \frac{k_{2,MEA}[MEA]([CO_2] - [CO_2]_e)}{1 + \frac{k_{-1}}{k_{H_2O}[H_2O] + k_{MEA}[MEA]}} + \frac{k_{2,MEA}[MEA]([CO_2] - [CO_2]_e)}{1 + \frac{k_{-1} + k_{H_2O}[H_2O]}{k_{MEA}[MEA]}} \quad (13)$$

The corresponding reaction rate constants in eqs 12 and 13 are presented in Table 1.

Table 1. Reaction Constant Used in eqs 12 and 13

reaction constant	unit	expression	ref
$k_{2,MEA}$	$m^3\ mol^{-1}\ s^{-1}$	$7.973 \times 10^9 \exp[-6243/T(K)]$	26
$((k_{2,MEA}k_{H_2O})/k_{-1})$	$m^6\ mol^{-2}\ s^{-1}$	$1.1 \exp[-3472/T(K)]$	26
$((k_{2,MEA}k_{MEA})/k_{-1})$	$m^6\ mol^{-2}\ s^{-1}$	$1.563 \times 10^8 \exp[-7544/T(K)]$	26

2.3. Vapor−Liquid Equilibrium (VLE) in MEA−H_2O−CO_2 System. The equilibrium CO_2 partial pressure and concentrations of all chemical species in MEA−H_2O−CO_2 system can be predicted by a VLE model presented by Aboudheir et al.[27] The model considers the following five reactions:

$$2H_2O \overset{K_W}{\longleftrightarrow} H_3O^+ + OH^- \quad (14a)$$

$$MEAH^+ + H_2O \overset{K_{MEAH+}}{\longleftrightarrow} MEA + H_3O^+ \quad (14b)$$

$$MEACOO^- + H_2O \overset{K_{MEACOO^-}}{\longleftrightarrow} MEA + HCO_3^- \quad (14c)$$

$$CO_2 + 2H_2O \overset{K_{CO_2}}{\longleftrightarrow} H_3O^+ + HCO_3^- \quad (14d)$$

$$HCO_3^- + H_2O \overset{K_{HCO_3^-}}{\longleftrightarrow} H_3O^+ + CO_3^{2-} \quad (14e)$$

The chemical equilibrium constants, which are a strong function of temperature T, usually can be expressed as

$$\ln K_{eq} = A + \frac{B}{T} + C \ln(T) + DT \quad (15)$$

where K_{eq} is the equilibrium constant for eqs 14a−14e; A, B, C, and D are adjustable parameters, which are available in Table 2, and T is the absolute temperature (given in Kelvin).

Table 2. Parameters *A*, *B*, *C*, and *D* for Equilibrium Constants in eq 15

reaction	*A*	*B*	*C*	*D*	ref
14a	132.899	−13445.9	−22.4773	0	28
14b	−3.0383	−7008.357	0	−0.0031348	29
14c	−0.52135	−2545.53	0	0	29
14d	231.465	−12092.1	−36.7816	0	30
14e	216.05	−12431.7	−35.4819	0	28

The relationship between gaseous CO_2 and CO_2 in the aqueous MEA−H_2O−CO_2 system can be expressed by Henry's Law,

$$P_{CO_2} = H_{CO_2,L} \times [CO_2] \quad (16)$$

where P_{CO_2} is the partial pressure of CO_2; $H_{CO_2,L}$ is the Henry's Law constant of CO_2 in aqueous MEA solution and its detailed calculation can be found in Appendix A.1; and $[CO_2]$ is the CO_2 concentration in the liquid phase.

Figures 3 and 4 present the comparison of predicted VLE data in this work and experimental data published in the literature. The predicted results show a good agreement with experimental data at CO_2 loadings of <0.6 mol CO_2/mol MEA. At CO_2 loadings of >0.6 mol CO_2/mol MEA, the predicted concentrations of $MEAH^+$ and HCO_3^- are higher than the literature values, as shown in Figure 4. However, in industrial practice, the maximum CO_2 loadings of MEA used are <0.55 mol CO_2/mol MEA, and in our work, the maximum CO_2 loading is 0.5 mol CO_2/mol MEA. Therefore, equilibrium CO_2 partial pressure and liquid-phase species concentrations predicted are acceptable in this work.

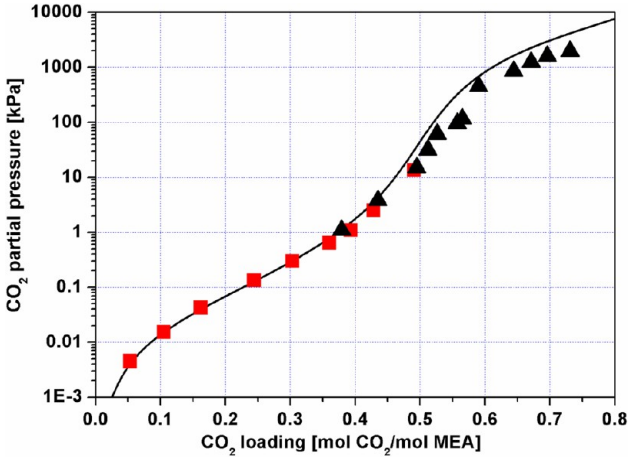

Figure 3. CO_2 equilibrium partial pressure over 30 wt % MEA at 333 K. (Legend: the line represents the predicted data, and the scattered data points represent the literature data ((■) Aronu et al.[31] and (▲) Shen et al.[32])

2.4. Physical Properties and Numerical Solutions. Some physical properties are needed to solve the above model equations. They include mass-transfer coefficients in the gas and liquid phase, Henry's Law constant, viscosities, dimensions of membrane contactor, etc. A representative of these values are listed in Table 3.

The partial differential equations related to the tube side under the appropriate boundary conditions were solved using Matlab software with the Method of Lines method for numerical solutions of these model equations. The length in

dx.doi.org/10.1021/ef401488c | Energy Fuels 2013, 27, 6887−6898

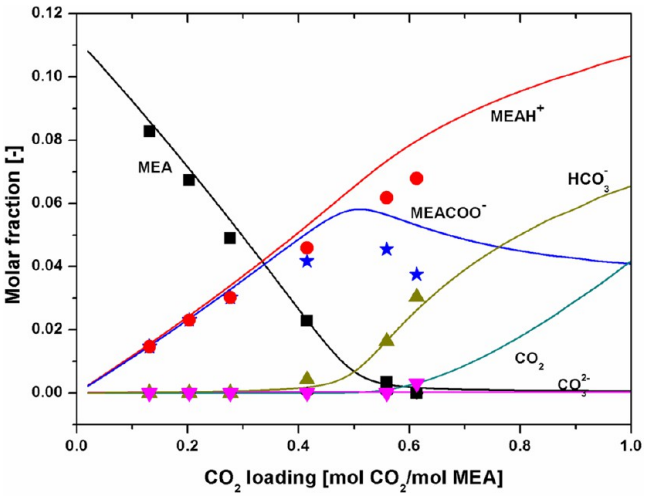

Figure 4. Molar concentration of chemical species in 30 wt % MEA at 333 K. (Legend: the line represents the predicted data, and the scattered data points reported by Böttinger et al.[33] ((■) MEA, (▲) HCO_3^-, (★) $MEACOO^-$, (▼) CO_2^{2-}, and (●) $MEAH^+$).

Table 3. Physical Properties and Dimensions of Hollow Fiber Membrane Contactor Used in the Model[a]

parameter	unit	value
	Membrane Dimensions	
d_i	m	4.00×10^{-4}
δ	m	4.00×10^{-5}
n		100
L	m	0.400
d_{module}	m	0.100
d_p	μm	0.100
	Physical Properties	
$D_{CO_2,L}$	$m^2\ s^{-1}$	3.86×10^{-9}
$D_{CO_2,G}$	$m^2\ s^{-1}$	1.44×10^{-5}
$D_{MEA,L}$	$m^2\ s^{-1}$	8.90×10^{-10}
D_{ig}^e	$m^2\ s^{-1}$	5.97×10^{-6}
$H_{CO_2,L}$	kPa m^3 $kmol^{-1}$	7807.97
η_L	Pa s	0.0008[b]

[a]Conditions: temperature = 353 K; regeneration pressure = 20 kPa; MEA concentration = 20 wt %). [b]Data taken from ref 34.

radial and axial directions are divided into 200 and 2500 grid points, respectively. The CO_2 loading of MEA solvent after regeneration can be determined by applying the mass balance equation along the fiber length.

3. RESULTS AND DISCUSSIONS

3.1. Model Validation. In order to validate the model developed in this work, a comparison of literature data and simulated results is conducted, as shown in Figure 5. $\Delta\alpha$ indicates the change of CO_2 loadings in MEA solvent after the membrane stripping process. The predicted results of $\Delta\alpha$ are in good agreement with the literature data at various liquid flow rates and two stripping temperatures. This demonstrates that the model for CO_2 membrane stripping process developed in this work is reliable.

3.2. Concentration Distribution of MEA and CO_2 in Membrane Fiber. A representative of concentration distribution of MEA and CO_2 in the lumen side of membrane contactor was predicted, as illustrated in Figure 6. MEA and

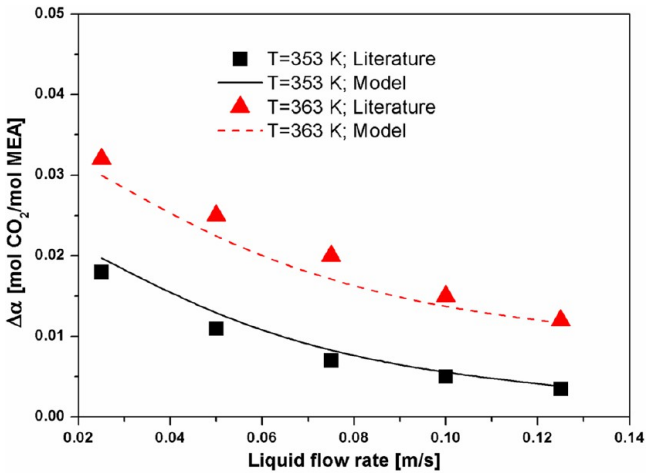

Figure 5. Comparison of simulated CO_2 loading changes with literature experimental data,[22] as a function of liquid flow rate at 353 and 363 K. (Conditions: CO_2-rich loading = 0.45 mol CO_2/mol MEA; MEA concentration = 2.5 mol/L; regeneration pressures = 110 kPa; and weeping gas velocity = 0.09 m/s.)

CO_2 concentrations at the inlet of membrane ($Z = 0$) are both assumed constant along the r-direction. Figure 6 shows that, for both MEA and CO_2, the concentration profiles are almost parabolic along the r-direction. The difference is that the mean MEA concentration increases along the membrane length, while the mean CO_2 concentration decreases. Figure 6 also shows that the concentrations of MEA and CO_2 vary significantly at the gas/liquid interface (r = 0.2 mm) with a relatively slight change of concentration in the zone near the axis of membrane ($r = 0$). This is because the reactions only occur at the gas/liquid interface, and the CO_2 desorption reaction rate is faster than diffusion rate in the liquid.

3.3. Effects of Key Operating Parameters on Regeneration Performance. In this section, the effects of key operating parameters, which includes liquid velocity, regeneration pressure, temperature, and sweeping steam flow rate, are predicted and discussed to further guide the optimization of membrane stripping process.

3.3.1. Effect of Liquid Velocity. The effect of liquid velocity on MEA regeneration performance is investigated, as shown in Figures 7 and 8. The CO_2 loading change after regeneration $\Delta\alpha$ and average CO_2 desorption flux N_{CO_2} are used to evaluate the regeneration performance. N_{CO_2} at a fiber length of z can be expressed as

$$N_{CO_2} = \frac{n\pi R^2 C_{MEA} V_L(\alpha_{rich} - \alpha_{lean})}{2n\pi Rz} = \frac{RC_{MEA}V_L(\alpha_{rich} - \alpha_{lean})}{2z} \quad (17)$$

in which V_L is the liquid velocity (in m/s); n is the fiber number; R is the radius of the membrane (in meters); $C_{MEA,f}$ is the concentration of fresh MEA solvent (in mol/m^3); α_{rich} is the CO_2-rich loading of MEA solvent; α_{lean} is the average CO_2 lean loading of MEA solvent at fiber length z.

Figure 7 shows that $\Delta\alpha$ is a decreasing function of liquid velocity. This is expected since a slower liquid velocity leads to an increase in residence time (reaction time) in membrane module and, thus, a higher $\Delta\alpha$. The similar result was also reported by Koonaphapdeelert et al.[22] and Fang et al.[19]

dx.doi.org/10.1021/ef401488c | Energy Fuels 2013, 27, 6887−6898

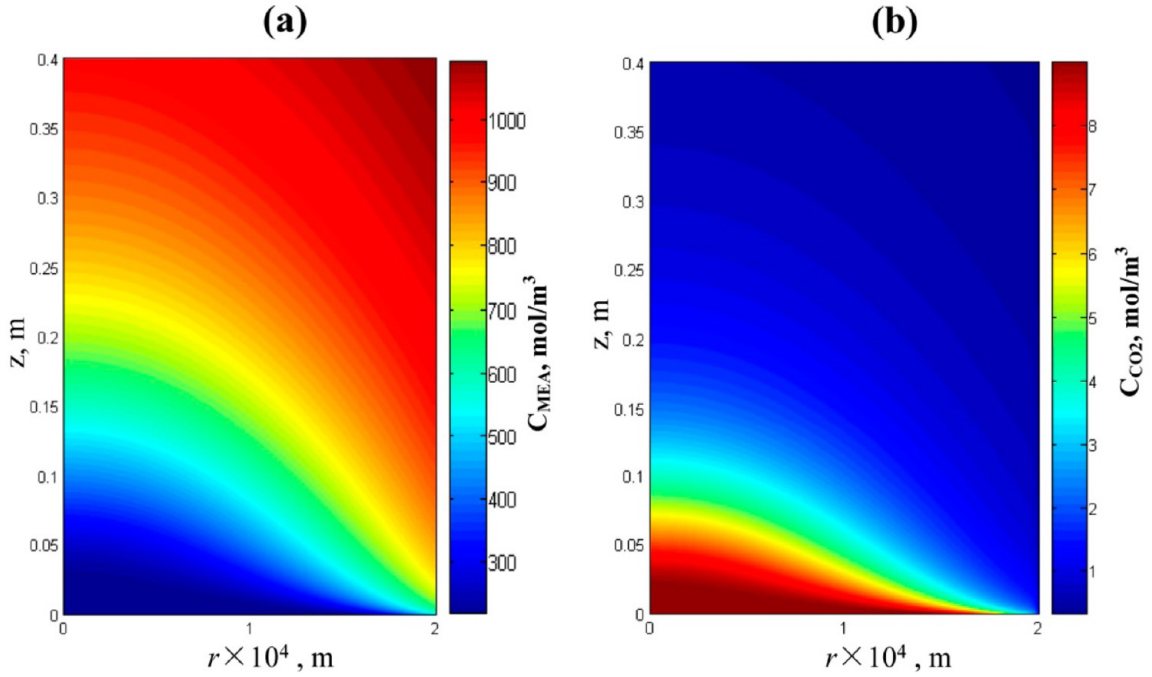

Figure 6. Representation of (a) MEA and (b) CO_2 concentration distribution in membrane fiber. (Conditions: α_{rich} is expressed in units of mol CO_2/mol MEA, MEA concentration = 20 wt %, regeneration temperature = 353 K, sweeping steam flow rate = 0.5 g/min, regeneration pressure = 20 kPa, liquid velocity = 0.01 m/s.)

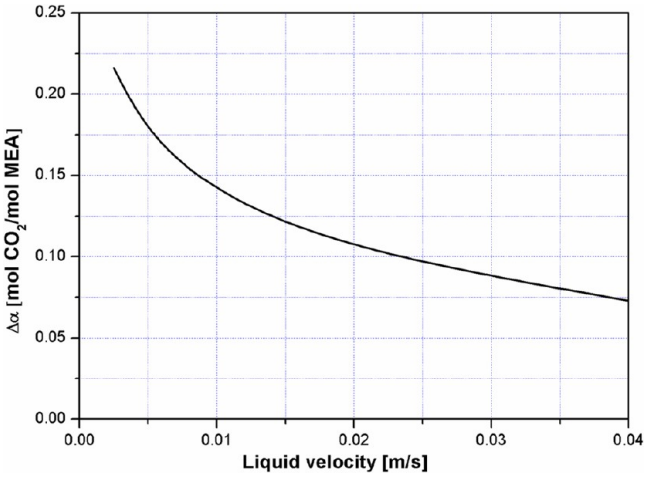

Figure 7. Effect of liquid velocity on $\Delta\alpha$. (Conditions: α_{rich} = 0.5 mol CO_2/mol MEA, MEA concentration = 20 wt %, regeneration temperature = 353 K, sweeping steam flow rate = 0.5 g/min, regeneration pressure = 20 kPa.)

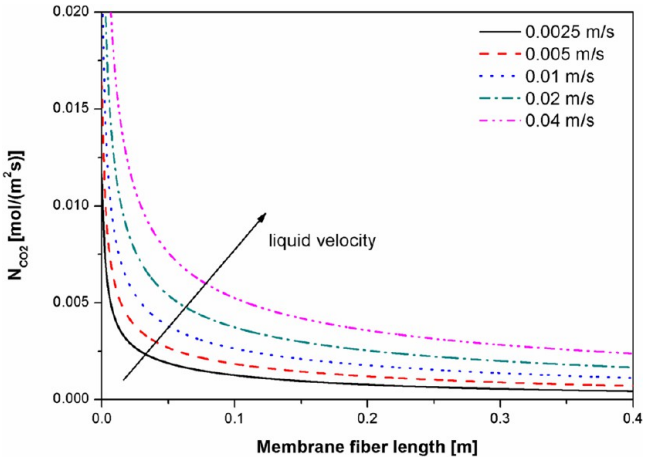

Figure 8. Profile of N_{CO_2} along the membrane module for different liquid velocities. (Conditions: α_{rich} = 0.5 mol CO_2/mol MEA, MEA concentration = 20 wt %, regeneration temperature = 353 K, sweeping steam flow rate = 0.5 g/min, regeneration pressure = 20 kPa.)

Equation 17 shows that CO_2 desorption flux is affected by both liquid velocity and CO_2 loading changes. Figure 8 reveals that a faster liquid velocity favors a high CO_2 desorption flux. This indicates that, as the liquid velocity increases, the loading change becomes small, but to a lesser extent of the increase of liquid velocity. As a result, the net impact of increase of liquid velocity is an increase in CO_2 desorption flux under the conditions studied. In addition, a decreasing trend of N_{CO_2} is found along the membrane fiber length at a fixed liquid flow rate and the extent of decrease gradually becomes smaller with the membrane length. This can be attributed to the difference in CO_2 desorption driving force, which usually can be expressed as $P_{CO_2,L} - P_{CO_2,G}$, along the length of the membrane. $P_{CO_2,L}$ and $P_{CO_2,G}$ are the CO_2 partial pressures in the liquid side and the gas side, respectively. Higher CO_2 desorption driving force will favor the CO_2 desorption flux. Along the membrane fiber, $P_{CO_2,L}$ is decreasing due to the decrease of CO_2 loading of MEA solution, and $P_{CO_2,G}$ is increasing due to more CO_2 desorption into gas phase. Consequently, CO_2 desorption driving force decrease along the membrane fiber, which result in a decreasing trend of N_{CO_2}. Moreover, at the end part of the membrane fiber, CO_2 equilibrium is closed between the liquid and gas sides; therefore, the decreasing trend in driving force is not as obvious as that at the beginning part.

For industrial practice, CO_2 capture is a CO_2 absorption–desorption cyclic process. A higher $\Delta\alpha$ value means a faster

dx.doi.org/10.1021/ef401488c | Energy Fuels 2013, 27, 6887–6898

CO_2 absorption rate in the absorber. From this view, slower liquid velocity will be preferred. However, it is at the cost of reducing N_{CO_2} and increasing size of membrane module. Moreover, from the regeneration energy consumption point of view, a $\Delta\alpha$ value that is too high or too low will both increase the regeneration energy.[35] Therefore, it is important to choose an appropriate liquid flow rate to account for the tradeoff between $\Delta\alpha$ and N_{CO_2}.

3.3.2. Effect of Regeneration Temperature. Figure 9 presents the influence of regeneration temperature on CO_2

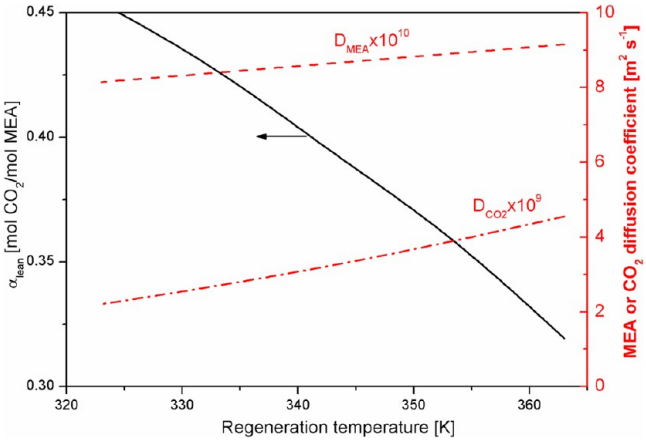

Figure 9. Effect of regeneration temperature on membrane stripping performance. (Conditions: α_{rich} = 0.5 mol CO_2/mol MEA, MEA concentration = 20 wt %, liquid velocity = 0.01 m/s, sweeping steam flow rate = 0.5 g/min, regeneration pressure = 20 kPa.)

membrane stripping performance. Temperature has a significant positive influence on CO_2 desorption. α_{lean} is an almost-linear decreasing function of regeneration temperature. This can be attributed to the effects of the temperature on diffusion coefficients and CO_2 solubility in liquid phase. As shown in Figure 9, the liquid-phase diffusion coefficients of CO_2 and MEA both increase with an increase in temperature, which will accelerate the penetration of solute CO_2 from the axis of the membrane fiber to the gas/liquid interface, leading to an increase of CO_2 desorption rate. Figure 10 shows the change of CO_2 equilibrium partial pressure over MEA solvent with the

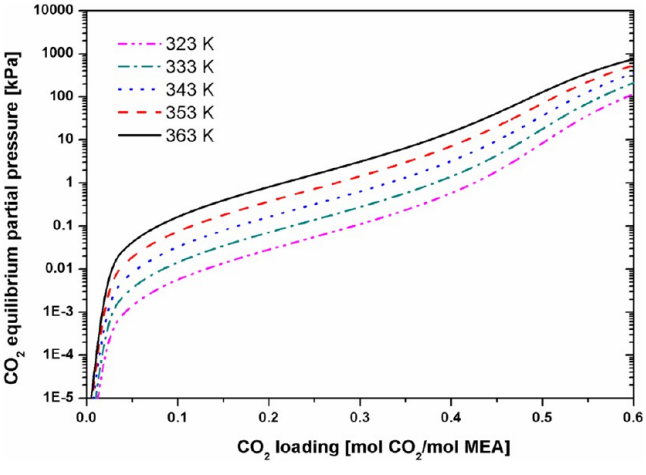

Figure 10. CO_2 equilibrium partial pressure over 20 wt % MEA at different temperatures.

temperature. Increasing temperature significantly increases CO_2 equilibrium partial pressure and, thus, the driving force for CO_2 desorption.

3.3.3. Effect of Regeneration Pressure. Figure 11 shows the change of $\Delta\alpha$ for two different operating modes (sweeping

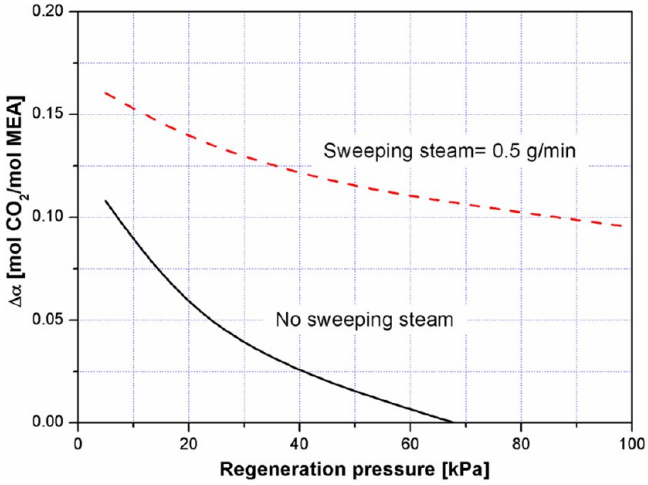

Figure 11. Effect of regeneration pressure on membrane stripping performance. (Conditions: α_{rich} = 0.5 mol CO_2/mol MEA, MEA concentration = 20 wt %, liquid velocity = 0.01 m/s, regeneration temperature = 353 K.)

steam = 0.5 g/min and no sweeping steam) under different regeneration pressures. For both modes, lowering regeneration pressure improves the CO_2 membrane stripping performance. The main reason is that lower regeneration pressure could contribute to the decrease in the partial pressure of CO_2 in the gas phase, which would promote the CO_2 desorption driving force. It is noteworthy that, with the existence of sweeping steam, $\Delta\alpha$ is obviously higher than that without sweeping steam at the same operating pressure. In addition, the sweeping steam operating mode presents less sensitivity to regeneration pressure than the no sweeping steam mode. This is because sweeping steam plays an important role in further reducing the CO_2 partial pressure in thegas phase. However, a decrease in regeneration pressure will lead to an increase of power cost on vacuum pump and risk of membrane wetting.[19] Therefore, very low regeneration pressure usually is not recommended in the practical operation.

3.3.4. Effect of Sweeping Steam Flow Rate. The change of $\Delta\alpha$ with sweeping steam flow rate in membrane stripping process is shown in Figure 12. It is clearly seen that $\Delta\alpha$ is an increasing function of the sweeping steam flow rate. As the sweeping steam flow rate increases from 0 to ~0.25 g/min, $\Delta\alpha$ increases significantly; however, when the sweeping steam flow rate is over 0.25 g/min, only a slight increase of $\Delta\alpha$ can be obtained with increasing sweeping steam flow rate. Consider the fact that more sweeping steam occurs at the cost of larger heat energy; therefore, the flow rate of sweeping steam is recommended around the transition point, ~0.25 g/min in this work, for the tradeoff between CO_2 desorption performance and heat consumption..

In order to gain a further understanding of the effect of sweeping steam on CO_2 membrane stripping performance, the profile of CO_2 partial pressure in gas phase along the membrane module is plotted in Figure 13. The CO_2 partial pressure in gas phase is increasing along the length of the

dx.doi.org/10.1021/ef401488c | *Energy Fuels* 2013, 27, 6887−6898

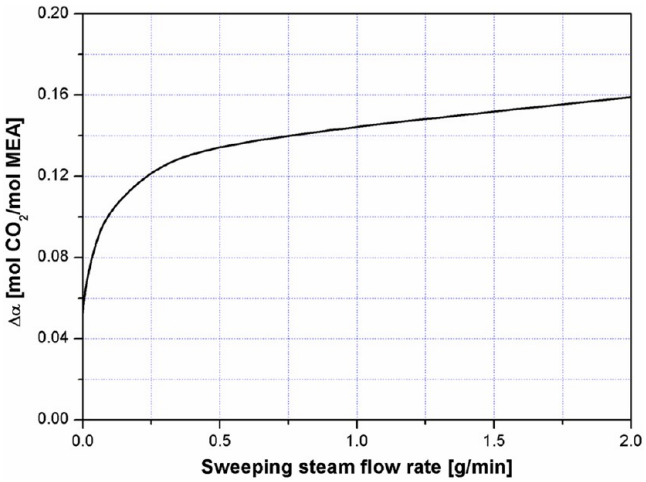

Figure 12. Effect of sweeping steam flow rate on CO_2 membrane stripping performance. (Conditions: α_{rich} = 0.5 mol CO_2/mol MEA, MEA concentration = 20 wt %, liquid velocity = 0.01 m/s, regeneration temperature = 353 K, regeneration pressure = 20 kPa.)

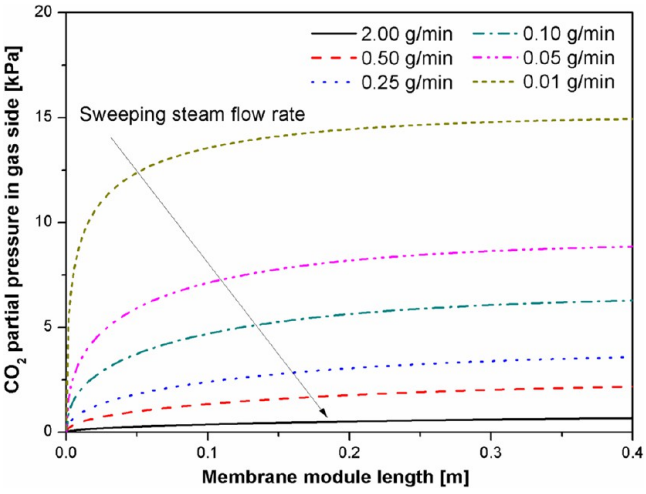

Figure 13. The profile of CO_2 partial pressure in gas phase along the membrane module under different sweeping steam flow rates. (α_{rich} = 0.5 mol CO_2/mol MEA, MEA concentration = 20 wt %, liquid velocity = 0.01 m/s, regeneration temperature = 353 K, and regeneration pressure = 20 kPa.)

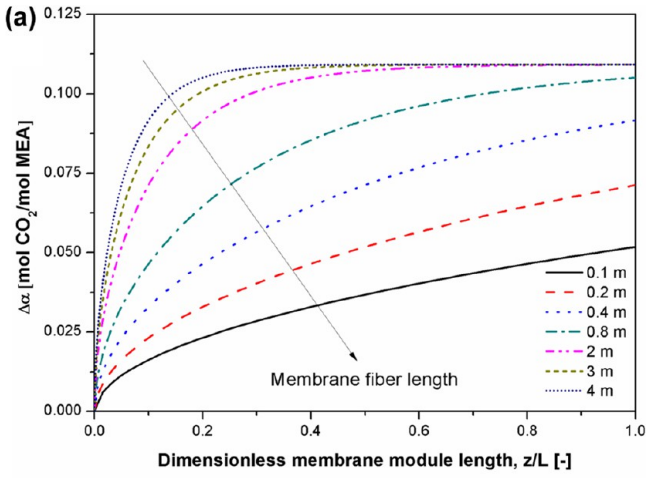

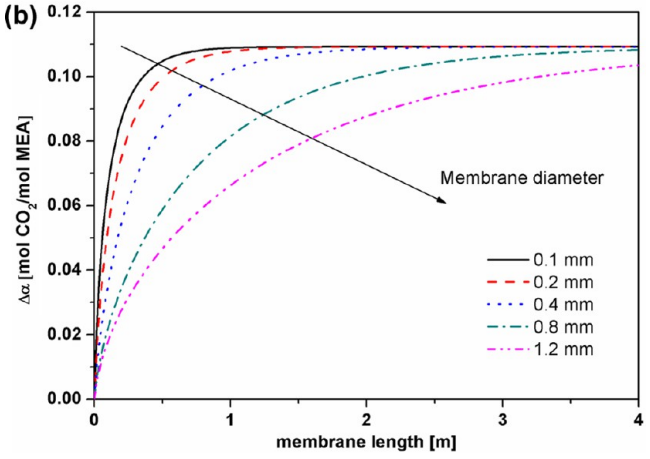

Figure 14. (a) Profiles of $\Delta\alpha$ along membrane module for different lengths of membranes. (Conditions: α_{rich} = 0.5 mol CO_2/mol MEA, MEA concentration = 20 wt %, liquid velocity = 0.01 m/s, sweeping steam flow rate = 0.1 g/min; regeneration temperature = 353 K, regeneration pressure = 20 kPa, membrane diameter = 0.4 mm, fiber number = 100, module diameter = 0.01 m.) (b) Profiles of $\Delta\alpha$ along membrane module for different diameters of membranes. (Conditions: α_{rich} = 0.5 mol CO_2/mol MEA, MEA concentration = 20 wt %, liquid velocity = 0.01 m/s, sweeping steam flow rate = 0.1 g/min; regeneration temperature = 353 K, regeneration pressure = 20 kPa, membrane length = 4 m, tube side cross section area = 1.26×10^{-5} m^2, module diameter = 0.01 m.)

membrane module due to the accumulation of CO_2 desorbed from liquid side to gas side with the module length. A higher flow rate of sweeping steam leads to a lower CO_2 partial pressure in gas phase, which will elevate the mass-transfer driving force of CO_2 desorption and promote the desorption of CO_2 in the membrane stripping process.

3.4. Effect of Membrane Fiber Length. The profiles of $\Delta\alpha$ along the membrane module for different lengths of membrane are presented in Figure 14a. A longer membrane will result in better membrane stripping performance. This is due to the increasing residence time of MEA solvent in membrane module with increasing membrane length. However, since the membrane length is long enough (e.g., 2 m), almost no change of $\Delta\alpha$ at module outlet (z/L = 1) can be found with further increases in membrane length, as a result of the thermodynamic limitation of absorbent. In addition, in the case of membrane length longer than 2 m, a flat profile of $\Delta\alpha$ can be seen in the end part of membrane module. It means that the end part of membrane is ineffective since CO_2 equilibrium is achieved between the gas and liquid phase in this part of membrane module. The effective membrane length was influenced by other membrane characteristics, such as membrane diameter. Figure 14b presents the profiles of $\Delta\alpha$ along the membrane module for different diameters of membranes. When the membrane diameter is 0.1 mm, the effective membrane length is ~0.5 m, and further increase in the membrane length will not lead to a significant increase of $\Delta\alpha$. As the membrane diameter increases, the effective length also increases. Therefore, in order to avoid the ineffective part of the membrane module, a shorter membrane module is preferred for thinner membranes.

3.5. Effect of Membrane Diameter. Figure 15 presents the effect of fiber membrane diameter on CO_2 membrane stripping performance. It is observed that $\Delta\alpha$ is a decreasing function of membrane diameter at a fixed liquid velocity. . The reason can be explained by the diffusion of MEA and CO_2 molecules in the liquid phase. Smaller diameter will shorten the

dx.doi.org/10.1021/ef401488c | Energy Fuels 2013, 27, 6887−6898

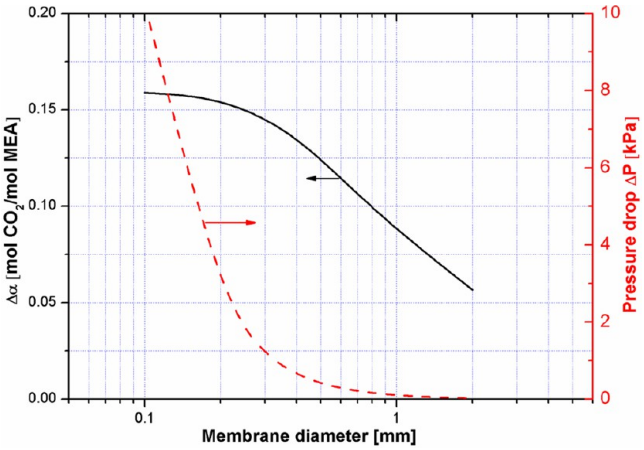

Figure 15. Effect of membrane diameter on CO_2 membrane stripping and pressure drop. (Conditions: α_{rich} = 0.5 mol CO_2/mol MEA, MEA concentration = 20 wt %, liquid velocity = 0.01 m/s, sweeping steam flow rate = 0.5 g/min; regeneration temperature = 353 K, regeneration pressure = 20 kPa, membrane length = 0.4 m, tube-side cross-sectional area = 1.26×10^{-5} m^2, and module diameter = 0.01 m.)

diffusion time of CO_2 from the axis of the membrane fiber to the gas/liquid interface. As the diameter is relatively small, $\Delta\alpha$ is decreasing slightly with the membrane diameter. This can be explained by Figure 16. Figure 16 plots the concentration

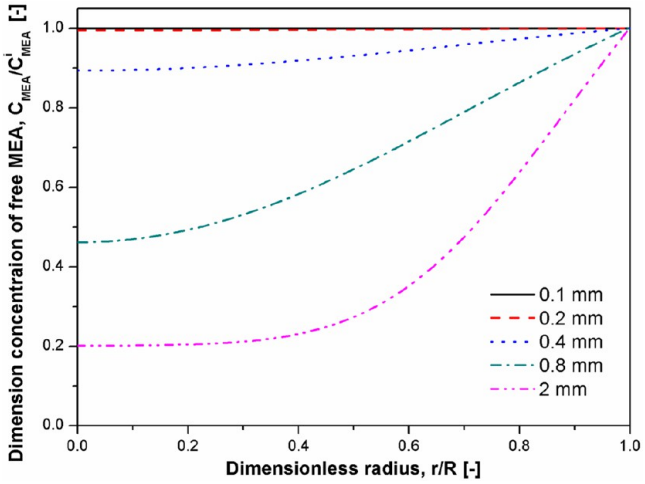

Figure 16. Concentration profiles of free MEA in the liquid phase along the membrane radial direction at the exit of the membrane module. (Conditions: α_{rich} = 0.5 mol CO_2/mol MEA, MEA concentration = 20 wt %, liquid velocity = 0.01 m/s, sweeping steam flow rate = 0.5 g/min; regeneration temperature = 353 K, regeneration pressure = 20 kPa, membrane length =0.4 m, tube side cross section area =$1.26 \times 10^{-5}$$m^2$, module diameter = 0.01 m.)

profiles of free MEA in the liquid phase along the membrane radial direction at the exit of the membrane module for different membrane diameters. For the membrane fiber with a small diameter, 0.1 mm, for example, the concentration gradient of free MEA between the liquid/gas interface (r/R = 1) and axis of membrane (r/R = 0) is very small. Therefore, the CO_2 desorption process in these membrane fibres can be considered to be reaction-controlled. With the increase of the membrane diameter, this concentration gradient becomes larger. It means that more free MEA is accumulated near the interface with increasing of membrane diameter. Consequently, the diffusion plays a more important role than the reaction, the CO_2 desorption process gradually changes from reaction-controlled to diffusion-controlled.

The pressure drop curve in liquid side with membrane diameter is also presented in Figure 15. Since the liquid in the lumen side is laminar flow, the theoretical pressure drop in the liquid side can be calculated using the Hagen−Poiseuille equation:

$$\Delta P = \frac{0.128\eta_L L Q_L}{\pi d_i^4} \tag{18}$$

where ΔP is the pressure drop (in kPa); L is the membrane length (given in meters); η_L is the dynamic viscosity of the liquid (given in units of Pa s); Q_L is the volumetric flow rate (m^3/s); d_i is the membrane inner diameter of the membrane fiber (in meters). The pressure drop increases sharply with decreasing diameter of membrane fiber. It means that more power is required to push liquid through the module with a smaller membrane diameter. Therefore, the membrane fiber with a small membrane diameter is not recommended, despite high CO_2 desorption performance.

3.6. Effect of Membrane Wetting Ratio. In the membrane stripping process, because of the vacuum operation on the gas side, the trans-membrane pressure is usually greater than that in the membrane absorption process. Moreover, long-term running of membrane could lead to a decrease in the contact angle of the membrane with a solvent and an increase in membrane pore size,[19] which will lower the minimum breakthrough pressure. Therefore, membrane wetting is a potential risk in membrane stripping process. The effects of membrane wetting ratio on CO_2 membrane stripping performance and membrane-gas combined mass-transfer coefficient are predicted, as shown in Figure 17. Membrane wetting has a very strong negative influence on CO_2 membrane stripping performance with α_{lean} decreasing suddenly once the membrane is wetted. For example, when the wetting ratio is only 10%, α_{lean} rises from an initial value of 0.362 mol CO_2/mol MEA to 0.462 mol CO_2/mol MEA. This can be explained by the fast decrease of k_{ex} with membrane wetting ratio, as shown in Figure 17.

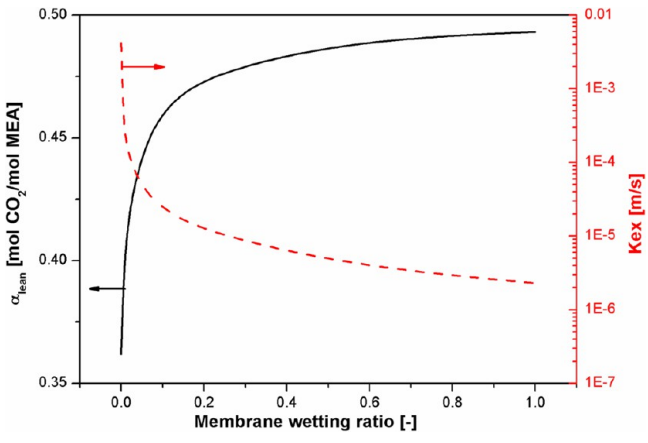

Figure 17. Predicted α_{lean} and k_{ex}, as a function of the membrane wetting ratio. (Conditions: α_{rich} expressed in terms of mol CO_2/mol MEA; MEA concentration = 20 wt %, liquid velocity = 0.01 m/s, sweeping steam flow rate = 0.1 g/min; regeneration temperature = 353 K, regeneration pressure = 20 kPa, membrane diameter = 0.4 mm, membrane length = 0.4 m; fiber number = 100, module diameter = 0.01 m.)

dx.doi.org/10.1021/ef401488c | Energy Fuels 2013, 27, 6887−6898

With further increases in the wetting ratio, the decrease of k_{ex} become smoothly, which results in a slow increase of α_{lean}. Therefore, it is crucial to ensure that the membranes used in CO_2 stripping process are operated without wetting.

4. CONCLUSIONS

We developed a two-dimensional (2-D) mathematical model to simulate the CO_2 desorption from 20 wt % MEA solvent with CO_2 loading of 0.5 CO_2/mol MEA in a hollow fiber membrane contactor. The modeling results agreed well with the experimental results from the literature. The effects of key operating parameters and structure characteristics of membrane fiber were investigated.

Lower liquid flows can decrease CO_2 lean loading, but at the cost of reducing CO_2 desorption flux. Increasing temperature has significant positive influence on improving CO_2 desorption performance. Lower regeneration pressure is in favor of improving the CO_2 membrane stripping performance. However, a decrease in regeneration pressure will lead to an increase of power cost on vacuum pump and risk of membrane wetting. Sweeping steam flow rate increases CO_2 desorption, but is only recommended at ~0.25 g/min, given the tradeoff between CO_2 desorption performance and heat consumption.

In terms of membrane fiber structure, we studied the influences of membrane length and membrane fiber diameter on CO_2 desorption. Results showed that increasing membrane's length will improve CO_2 stripping performance, but not infinitely, because of the thermodynamic limitations of the absorbent, and shorter membrane module is preferred for athinner membrane. However, because of the thermodynamic limitations of the absorbent, a very long membrane is not recommended. The change of CO_2 loading after regeneration is a decreasing function of membrane diameter.

Finally, to predict the influence of membrane wetting on CO_2 stripping performance, the change of CO_2 lean loading with wetting ratio was investigated. Membrane wetting significantly deteriorates CO_2 membrane desorption performance, with CO_2 lean loading increasing suddenly once the membrane is wetted.

APPENDIX

A.1. CO_2 Diffusion Coefficients

A.1.1. CO_2 Diffusion Coefficient in the Liquid Phase. The CO_2 diffusivity in MEA solvent can be predicted by the analogy of N_2O diffusivity in solution[36]

$$D_{CO_2,L} = D_{N_2O,L}\left(\frac{D_{CO_2,W}}{D_{N_2O,L}}\right) \tag{A1}$$

where $D_{CO_2,L}$ and $D_{CO_2,W}$ are CO_2 diffusivities in MEA solvent and pure water, respectively; $D_{N_2O,L}$ and $D_{N_2O,W}$ are N_2O diffusivities in MEA solvent and pure water, respectively.

The parameters $D_{CO_2,W}$ and $D_{N_2O,W}$ can be expressed as[37]

$$D_{CO_2,W} = 2.35 \times 10^{-6} \exp\left(\frac{-2119}{T}\right) \tag{A2}$$

$$D_{N_2O,W} = 5.07 \times 10^{-6} \exp\left(\frac{-2371}{T}\right) \tag{A3}$$

$D_{N_2O,L}$ is calculated according to the modified Stokes−Einstein relation:

$$D_{N_2O,L}\eta_L^{0.6} = D_{N_2O,W}\eta_W^{0.6} \tag{A4}$$

where η_L and η_W are the viscosities of MEA solution and water, respectively.

A.1.2. CO_2 Diffusion Coefficient in the Gas Phase. When gas B diffuses into gas F, the diffusivity of gas B can be calculated by the Maxwell−Gilliland equation:[38]

$$D_{B,F} = \frac{4.36 \times 10^{-5} T_G^{3/2} \sqrt{\frac{1}{M_B} + \frac{1}{M_F}}}{P(\nu_F^{1/3} + \nu_B^{1/3})^2} \tag{A5}$$

where T_G is the gas-phase temperature ; M_B and M_F are the molecular weight of gas B and F, respectively (in g/mol); P is the pressure in the gas phase (kPa); ν_B and ν_F are the molecule volume of gas B and F, respectively (cm^3/mol).

A.1.3. Effective Diffusion Coefficient of CO_2 in the Membrane. The diffusion through membrane is the combination of molecular diffusion and Knudsen diffusion. The calculation of effective diffusion coefficient of CO_2 D_{ig}^e can be determined by

$$\frac{1}{D_{ig}^e} = \frac{1}{D_{ig}^m} + \frac{1}{D_{ig}^k} \tag{A6}$$

in which D_{ig}^m and D_{ig}^k are the molecular and Knudsen diffusion coefficient of CO_2, respectively.

D_{ig}^m is calculated from the kinetic gas theory:[39]

$$D_{ig}^m = 1200\left(\frac{\bar{R}T}{MP}\right)\left(\frac{\Omega_\mu}{\Omega_D}\right)\mu \tag{A7}$$

where $\bar{R}$ is the ideal gas constant, M is the gas molecular weight, and μ is the gas dynamic viscosity (in Pa s). P is gas pressure (in kPa). Ω_u and Ω_D are viscosity collision integral and diffusion collision integral, respectively:

$$\Omega_D = \frac{1.6036}{(\bar{T})^{0.1561}} + \frac{0.193}{\exp(0.47635\bar{T})} + \frac{1.03587}{\exp(1.52996\bar{T})} + \frac{1.76474}{\exp(3.89411\bar{T})} \tag{A8}$$

$$\Omega_\mu = \frac{1.16145}{(\bar{T})^{0.14875}} + \frac{0.52487}{\exp(0.7732\bar{T})} + \frac{2.16178}{\exp(2.43787\bar{T})} \tag{A9}$$

$\bar{T}$ is the dimensionless temperature ($\bar{T} = \kappa T/\varepsilon$); κ is the Boltzmann constant; and ε is the parameter of Stockmayer potential, which can be estimated using the critical temperature.

D_{ig}^k can be calculated using the following equation:[40]

$$D_{ig}^k = 48.5 d_p \sqrt{\frac{T_G}{M}} \tag{A10}$$

where T_G is the gas temperature, M is the molecular weight of gas, and d_p is the mean pore diameter.

A.2. MEA Diffusion Coefficient in the Liquid Phase

The diffusion coefficient of MEA in water can be determined via the following correlation:[37]

$$D_{MEA,W} = 2.5 \times 10^{-10}\left(\frac{M}{\rho}\right)^{-0.54} \tag{A11}$$

in which M is the molar weight of MEA and ρ is the density of MEA.

dx.doi.org/10.1021/ef401488c | Energy Fuels 2013, 27, 6887−6898

The diffusion coefficient of MEA molecule in MEA solution were correlated for viscosity and temperature using the modified Stokes−Einstein relation:[41]

$$D_{\mathrm{MEA,L}} = D_{\mathrm{MEA,W}}\left(\frac{T}{273}\right)\left(\frac{\eta_{\mathrm{W}}}{\eta_{\mathrm{L}}}\right)^{0.6} \quad \text{(A12)}$$

A.3. Henry's Constant

Henry's constant of CO_2 in MEA solution can also be calculated via the N_2O analogy,

$$H_{\mathrm{CO_2,L}} = H_{\mathrm{N_2O,L}}\left(\frac{H_{\mathrm{CO_2,W}}}{H_{\mathrm{N_2O,W}}}\right) \quad \text{(A13)}$$

in which $H_{\mathrm{N_2O,L}}$ is the Henry constant of N_2O in aqueous amine. Henry's constant of CO_2 and N_2O in water ($H_{\mathrm{CO_2,W}}$ and $H_{\mathrm{N_2O,W}}$, respectively) can be determined in the following equations, provided by Versteeg et al.:[37]

$$H_{\mathrm{CO_2,W}} = 2.82 \times 10^6 \exp\left(\frac{-2044}{T_{\mathrm{L}}}\right) \quad \text{(A14)}$$

$$H_{\mathrm{N_2O,W}} = 8.55 \times 10^6 \exp\left(\frac{-2284}{T_{\mathrm{L}}}\right) \quad \text{(A15)}$$

Wang et al.[42] proposed the solubility of N_2O in pure amine solvent as follows:

$$H_{\mathrm{N_2O-pure\ amine}} = d_1 \exp\left(\frac{d_2}{T}\right) \quad \text{(A16)}$$

in which d_1 and d_2 are the parameter for calculating N_2O solubility in pure amine and were reported by Wang et al.[42]

The N_2O solubility in the aqueous amine can be described by a semi-empirical model, by correlating excess Henry's coefficient presented as follows:[43]

$$X = \ln H_{\mathrm{N_2O,L}} - \sum_{i=1}^{n} \Phi_i \ln H_{\mathrm{N_2O},i} \quad \text{(A17)}$$

In this equation, X is the excess Henry's coefficient, and Φ_i is the volume fraction of the ith solvent.

AUTHOR INFORMATION

Corresponding Author

*Tel.: 86-571-87952803. Fax: 86-571-87951616. E-mail: mxfang@zju.edu.cn.

Notes

The authors declare no competing financial interest.

ACKNOWLEDGMENTS

This work was financially supported by the National Natural Science Foundation of China (Nos. 51076139 and 51276161) and Zhejiang Province Key Science Inovation Team Project (No. 2009R50048). Z.W. is grateful for financial support from the Australian Government under the Australia−China Joint Coordination Group on Clean Coal Technology Partnership Fund, which allows him to carry out part of work in CSIRO.

NOMENCLATURE

C = molar concentration [mol m^{-3}]
d_p = pore diameter [μm]
d_i = membrane inner diameter [m]
d_h = hydraulic diameter of shell side [m]
D = diffusion coefficient [m^2 s^{-1}]
D_{ig}^{e} = effective diffusion coefficient of CO_2 in membrane [m^2 s^{-1}]
D_{ig}^{m} = molecular diffusion coefficient of CO_2 [m^2 s^{-1}]
D_{ig}^{k} = Knudsen diffusion coefficient of CO_2 [m^2 s^{-1}]
H = Henry's constant [kPa m^3 kmol^{-1}]
k_2 = second-order forward reaction rate constant [m^3 mol^{-1} s^{-1}]
k_{-1} = reverse first-order reaction rate constant [s^{-1}]
k_b = second-order forward reaction rate constant for base b [m^3 mol^{-1} s^{-1}]
k_m = mass-transfer coefficient in membrane phase [m s^{-1}]
k_g = mass-transfer coefficient in gas phase [m s^{-1}]
L = membrane fiber length [m]
m = distribution coefficient between liquid and gas [-]
M = molecular weight [g mol^{-1}]
n = number of membrane fibers
N_{CO_2} = CO_2 desorption flux [mol m^{-2} s^{-1}]
P = pressure [kPa]
ΔP = pressure drop [kPa]
Q_L = volumetric flow rate [m^3 s^{-1}]
V = velocity [m s^{-1}]
$\overline{V}$ = liquid mean velocity [m s^{-1}]
r = radial coordinate
r_{CO_2} = CO_2 reaction rate [mol m^{-3} s^{-1}]
r_{MEA} = MEA reaction rate [mol m^{-3}s^{-1}]
R_i = inner radius of membrane fiber [m]
T = temperature [K]
$\overline{T}$ = dimensionless temperature
ν = molecular volume of gas [cm^3 mol^{-1}]
X = Excess Henry's coefficient
z = axial coordinate
Re = Reynolds number
Sc = Schmidt number
Sh = Sherwood number

Greek Symbols

α = CO_2 loading [mol CO_2/mol MEA]
δ = membrane thickness [m]
τ = membrane tortuosity [m^{-2}]
ς = membrane porosity
ϕ = membrane pore wetting ratio
φ = packing density
κ = Boltzmann's constant [J K^{-1}]
η = dynamic viscosity [Pa s]
μ = viscosity of gas [Pa s]
κ = Boltzmann's constant [J K^{-1}]
ε = Stockmayer potential parameter [J]
Ω_μ = viscosity collision integral
Ω_D = diffusion collision integral
Φ_i = volume fraction of the ith solvent

Subscripts

ex = external
0 = initial time
e = equilibrium
f = fresh
M = membrane
G = gas
L = liquid
W = water

REFERENCES

(1) Kerr, R. A. *Science* **2006**, *312*, 1854.
(2) Tan, C. S.; Chen, J. E. *Sep. Purif. Technol.* **2006**, *49*, 174−180.
(3) Wang, M.; Lawal, A.; Stephenson, P.; Sidders, J.; Ramshaw, C. *Chem. Eng. Res. Des.* **2011**, *89*, 1609−1624.
(4) Rao, A. B.; Rubin, E. S. *Environ. Sci. Technol.* **2002**, *36*, 4467−4475.
(5) Rocelle, G. T. *Science* **2009**, *325*, 1652−1654.
(6) Mimura, T.; Simayoshi, H.; Suda, T.; Iijima, M.; Mituoka, S. *Energy Convers. Manage.* **1997**, *38*, S57−S62.
(7) Merkel, T. C.; Lin, H.; Wei, X.; Baker, R. *J. Membr. Sci.* **2010**, *359*, 126−139.
(8) Oyenekan, B. A.; Rochelle, G. T. *Ind. Eng. Chem. Res.* **2006**, *45*, 2457−2464.
(9) Van Wagener, D. H.; Rochelle, G. T. *Energy Procedia* **2011**, *4*, 1323−1330.
(10) Gabelman, A.; Hwang, S. T. *J. Membr. Sci.* **1999**, *159*, 61−106.
(11) Mansourizadeh, A. *Chem. Eng. Res. Des.* **2012**, *90*, 555−562.
(12) Li, J. L.; Chen, B. H. *Sep. Purif. Technol.* **2005**, *41*, 109−122.
(13) Rangwala, H. A. *J. Membr. Sci.* **1996**, *112*, 229−240.
(14) Matsumoto, H.; Kitamura, H.; Kamata, T.; Ishibashi, M.; Ota, H.; Akutsu, N. *J. Chem. Eng. Jpn.* **1995**, *28*, 125−128.
(15) Yan, S.; Fang, M.; Zhang, W.; Zhong, W.; Luo, Z.; Cen, K. *Energy Convers. Manage.* **2008**, *49*, 3188−3197.
(16) Mansourizadeh, A.; Ismail, A. F. *J. Hazard. Mater.* **2009**, *171*, 38−53.
(17) Kosaraju, P.; Kovvali, A. S.; Korikov, A.; Sirkar, K. K. *Ind. Eng. Chem. Res.* **2005**, *44*, 1250−1258.
(18) Khaisri, S.; deMontigny, D.; Tontiwachwuthikul, P.; Jiraratananon, R. *J. Membr. Sci.* **2011**, *376*, 110−118.
(19) Fang, M.; Wang, Z.; Yan, S.; Cen, Q.; Luo, Z. *Int. J. Greenhouse Gas Control* **2012**, *9*, 507−521.
(20) Wang, Z.; Fang, M.; Pan, Y.; Yan, S. P.; Luo, Z. Y. *Chem. Eng. Sci.* **2013**, *93*, 238−249.
(21) Simioni, M.; Kentish, S. E.; Stevens, G. W. *J. Membr. Sci.* **2011**, *378*, 18−27.
(22) Koonaphapdeelert, S.; Wu, Z. T.; Li, K. *Chem. Eng. Sci.* **2009**, *64*, 1−8.
(23) Mavroudi, M.; Kaldis, S. P.; Sakellaropoulos, G. P. *J. Membr. Sci.* **2006**, *272*, 103−115.
(24) Prasad, P.; Sirkar, K. K. *AIChE J.* **1988**, *34*, 177−188.
(25) Caplow, M. *J. Am. Chem. Soc.* **1968**, *90*, 6795−6803.
(26) Liao, C.; Li, M. *Chem. Eng. Sci.* **2002**, *57*, 4569−4582.
(27) Aboudheir, A.; Tontiwachwuthikul, P.; Chakma, A.; Idem, R. *Chem. Eng. Sci.* **2003**, *58*, 5195−5210.
(28) Edwards, T. J.; Maurer, G.; Newman, J.; Prausnitz, J. M. *AIChE J.* **1978**, *24*, 966−976.
(29) *ASPEN Plus, V7.2*; Aspen Technology: Burlington, MA, 2010.
(30) Maurer, G. *ACS Symp. Ser.* **1980**, *133*, 139−172.
(31) Aronu, U. E.; Gondal, S.; Hessen, E. T.; Haug-Warberg, T.; Hartono, A.; Hoff, K. A.; Svendsen, H. F. *Chem. Eng. Sci.* **2011**, *66*, 6393−6406.
(32) Shen, K. P.; Li, M. H. *J. Chem. Eng. Data* **1992**, *37*, 96−100.
(33) Böttinger, W.; Maiwald, M.; Hasse, H. *Fluid Phase Equilib.* **2008**, *263*, 131−143.
(34) Amundsen, T. G.; Øi, L. E.; Eimer, D. A. *J. Chem. Eng. Data* **2009**, *54*, 3096−3100.
(35) Oyenekan, B. A.; Rochelle, G. T. *Ind. Eng. Chem. Res.* **2006**, *45*, 2457−2464.
(36) Versteeg, G. F.; van Swaaij, W. P. M. *J. Chem. Eng. Data* **1988**, *33*, 29−34.
(37) Glasscock, D. A. *Modeling and Experimental Study of Carbon Dioxide Absorption in Aqueous Alkanolamines*, Ph.D. Thesis Dissertation; University of Texas at Austin, Austin, TX, 1990.
(38) Gilliland, E. R. *Ind. Eng. Chem.* **1934**, *26*, 681−685.
(39) Reid, R. C.; Prausnitz, J. M.; Sherwood, T. K. *The Properties of Gases and Liquids*, 3rd Edition; McGraw−Hill: New York, 1977.
(40) Cussler, E. L. *Diffusion: Mass Transfer in Fluid Systems*, 3rd Edition; Cambridge University Press: New York, 2009.
(41) Mandal, B. P.; Kundu, M.; Bandyopadhyay, S. S. *J. Chem. Eng. Data* **2003**, *48*, 703−707.
(42) Wang, Y. W.; Xu, S.; Otto, F. D.; Mather, A. E. *Chem. Eng. J.* **1992**, *48*, 31−40.
(43) Bensetiti, Z.; Iliuta, I.; Larachi, F.; Grandjean, B. P. A. *Ind. Eng. Chem. Res.* **1999**, *38*, 328−332.